Evaluation of urban heat island mitigation strategies for the Kansas City region

Seongeun Jeong, Dev Millstein, Ronnen Levinson

Heat Island Group, Energy Technologies Area, Lawrence Berkeley National Laboratory, Berkeley, CA

Abstract

We evaluate two mitigation strategies for urban heat island in the Kansas City Metropolitan Area (KCMA). Using the Weather Research and Forecasting (WRF) model, we assess the potential benefits of highly reflective cool roofs and urban irrigation on urban air temperature in typical summer conditions between 2011 and 2015, and also during six of the strongest historical heat wave events over the past 12 years (2005 – 2016). Under the typical summer conditions, we simulate near-surface (2-m) air temperature for 10 summer weeks, finding average daytime (07:00 – 19:00 local standard time) temperature reductions of 0.08 and 0.28 °C for cool roofs and urban irrigation, respectively. During the six heat-wave episodes, we also find similar daytime temperature reductions of 0.02 and 0.26 °C for the two scenarios compared to those of the typical summer conditions. Our results suggest that urban irrigation can be more efficient than cool roofs in mitigating the urban heat island in metropolitan regions where the majority of the urban land cover is comprised of areas with low urban (i.e., non-vegetated) fractions. Finally, we find the alteration of land surface conditions due to enhanced roof albedos impacts local meteorology and precipitation patterns within the WRF simulation, in particular during the heat wave periods. Further research would be necessary to determine the robustness of this last finding.

1. Introduction

Temperatures in urban regions are increasing due to a combination of global climate change and local factors such as the use of heat-trapping materials and anthropogenic heat sources [Hassid, S et al., 2000; Miller et al., 2008; Salamanca et al., 2013]. A recent study in North America suggests that urban expansion alone can increase regional temperature at a level similar to warming due to the increase of greenhouse gases in the atmosphere [Georgescu et al., 2014]. In addition, temperature increase in urbanized areas is known to be a source of air quality problems [Nazaroff, 2013] and heat-related public health problems [Luber and McGeehin, 2008; Li and Bou-Zeid, 2013; Yang et al., 2013].

Carefully planned urban growth strategies may provide an opportunity to mitigate urban heat stress. Increasing the solar reflectance (albedo) of roofs can cool buildings, reducing air conditioning use and lowering urban air temperatures [Parker and Barkaszi, 1997; Akbari et al., 1999; Levinson et al., 2005; 2010, Vahmani et al., 2016]. A second strategy to mitigate urban heat stress is to irrigate the urban vegetated landscape. Urban irrigation can reduce urban

temperature by increasing evaporative cooling of the air [Vahmani and Hogue, 2015; Vahmani and Ban-Weiss, 2016].

In this report, we evaluate potential temperature reductions from both highly reflective "cool" roofs and urban irrigation in the Kansas City Metropolitan Area (KCMA), a major metropolitan area in the Midwestern region of the United States. We examine air temperature reductions from each of the two mitigation strategies. We also show potential impact of changes in the land surface and near-surface atmospheric conditions on air temperature over the study domain.

This study tests the impacts of full, idealized, implementation of the mitigation strategies – in other words, all roofs are switched to cool roofs and all vegetated areas are irrigated. In practice, neither all roofs nor all vegetated areas would be treated in this manner. In the case of urban irrigation, urban irrigation serves as a surrogate for a strategy that supports stormwater infiltration practices via green infrastructure.

2. Method

2.1. WRF Urban Canopy Model

We use the Weather Research and Forecasting (WRF) model (version 3.8, [Skamarock et al., 2008]) to simulate different urban heat island mitigation strategies. The WRF model has been widely used for numerical weather prediction and also to investigate issues related to regional climate, atmospheric transport, air quality, and water resources [e.g., Chen et al., 2011; Jeong et al., 2016; 2017; Vahmani and Ban-Weiss, 2016; Bagley et al., 2017]. We use the single-layer urban canopy model (SLUCM, Kusaka et al., 2001; Kusaka and Kimura, 2004) to represent the urban physics. We use the Noah land surface model (LSM) [Chen and Dudhia, 2001], following a number of urban modeling studies (e.g., Millstein and Menon, 2011; Salamanca et al., 2013; Cao et al., 2015; Vahmani and Ban-Weiss, 2016). In the coupled WRF-SLUCM model, SLUCM is used to simulate the surface energy balance for the urban portion of each grid cell while the Noah LSM is used for the vegetated portion. WRF-SLUCM parameterizes the influence of urban canyons and building and pavement thermal properties on the surface energy budget [Chen et al., 2011].

The main physical options for WRF-SLCUM simulations in this study are set as follows: (1) radiation: RRTM scheme [Mlawer et al., 1997] for the longwave and Dudhia scheme [Dudhia, 1989] for the shortwave; (2) planetary boundary layer: UW (Bretherton and Park) scheme [Bretherton and Park, 2009]; (3) microphysics: Morrison double-moment scheme [Morrison et al., 2009]; and (4) cumulus: Grell-Freitas ensemble scheme [Grell and Freitas, 2014]. The initial and boundary meteorology conditions for WRF are provided by the North American Regional Reanalysis (NARR, Mesinger et al., 2006). A two-way nesting scheme for the three-level domains (13.5, 4.5 and 1.5 km) is used for the meteorology simulations (Figure 1). The atmosphere is divided into a total of 30 levels.

Figure 1 shows the entire modeling domain and the 1.5-km inner domain that includes KCMA. The National Land Cover Data (NLCD; Fry et al., 2011), which provides forty land cover types, is utilized to define land type in the study domains (Figure 1). We adopt the default urban

fractions of 50%, 90%, 95% for the three urban types: low, medium and high development intensity, respectively. For a given model gird cell, the urban fraction is the ratio of the urban (pavement and buildings) portion to the total area of the grid cell. To better represent the urban canopy in WRF simulations, we use the urban parameter data (e.g., mean building height) from National Urban Database and Access Portal Tool (NUDAPT, Ching et al., 2009). Because the NUDAPT dataset was available only for the urban core area of KCMA, we extrapolate the existing dataset to cover the entire KCMA. In this extrapolation, we calculated median values by development intensity (i.e., low, medium, and high) from the available NUDAPT dataset and applied them to non-NUDAPT areas.

Using a spin-up of 18 hours, we simulate meteorological variables including 2-m temperature in typical summer conditions between 2011 and 2015 and during six of the strongest historical heat wave events over the past 12 years (2005 – 2016; see the supplemental Figure S1 for selected heat wave periods). The diagnostic 2-m temperature (hereafter air temperature) variable in WRF-SLCUM represents an air temperature near the height of the urban canopy [Li and Bou-Zeid, 2014].

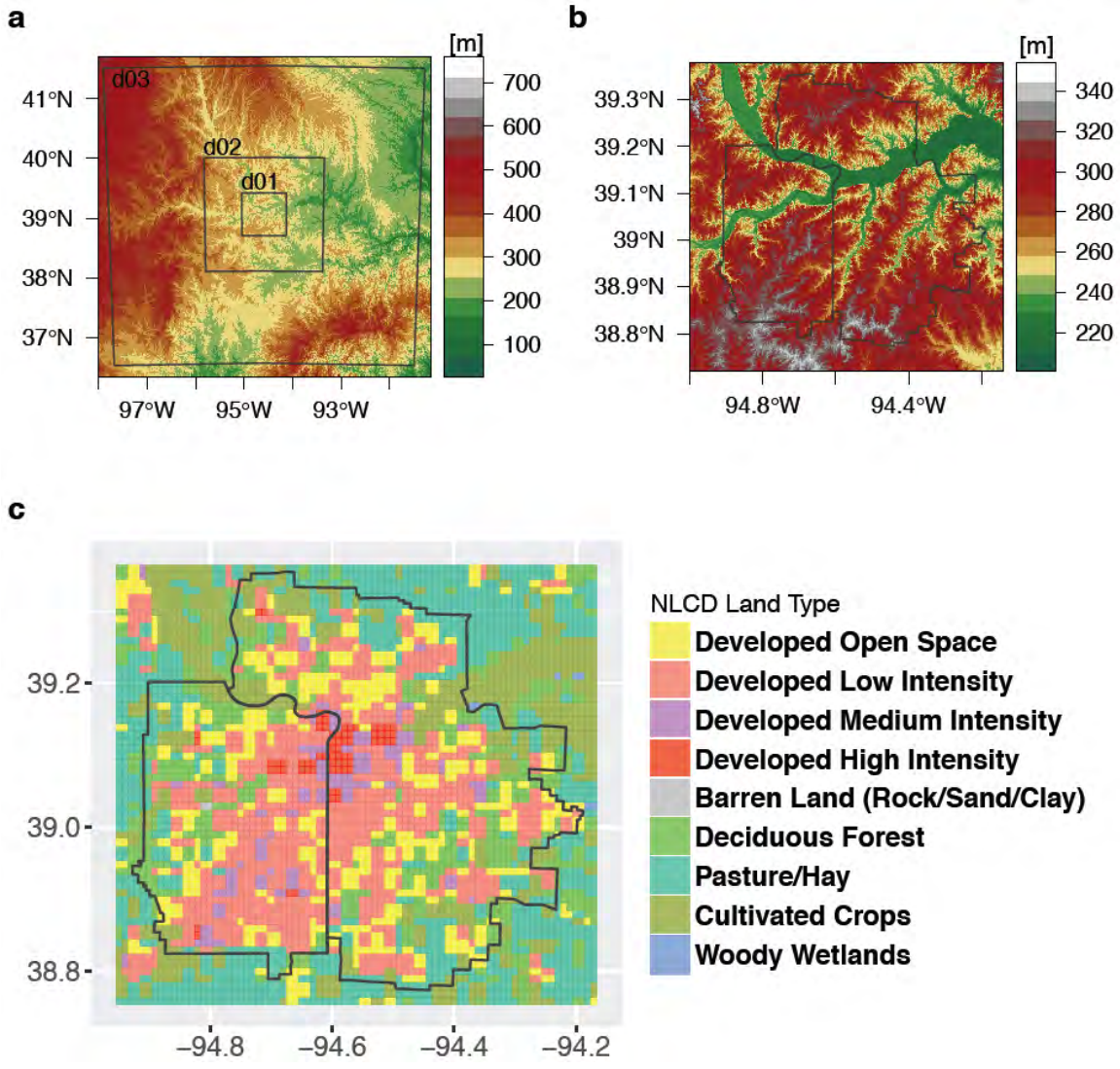

Figure 1. Maps showing (a) elevation of the entire modeling domain, at horizontal resolution of 1 arc-second (~30 m) [National Map, 2017]; (b) elevation of inner modeling domain; and (c) land type [Fry et al., 2011]. Boxes d01, d02, and d03 in panel (a) represent WRF modeling outer (d01) and nested (d02 and d03) domains, while the boundary (black solid line) in panels (b) and (c) represents the urbanized area in the Kansas City metropolitan region from the 2000 U.S. Census [Mid-America Regional Council, 2017].

2.2. Mitigation Strategies for WRF Simulations

We run a series of simulations to evaluate urban temperature reductions in KCMA upon raising roof albedo, and increasing urban irrigation. We ran 10 week long simulations representing typical summer conditions, selecting the 15th – 21st of July and August in 2011 – 2015. Separately, we identified and simulated six of the strongest historical heat-wave events over the past decade (2005 – 2016). For historic heat waves, we identified the episodic heat wave periods using measured near-surface air temperature data at the C. R. Wheeler Downtown Airport located in the urban area of KCMA (supplemental Figure S1), which are available from the Integrated Surface Database (ISD) of NOAA's National Centers for Environmental Information (NCEI, 2017). We selected six heatwave episodes by finding the periods with the highest seven-day moving average temperatures during 2005 – 2016 (supplemental Figure S1). For 2012, we identified two heat waves but selected the stronger episode in early July.

For each 7-day episode, we conduct independent WRF simulations for two mitigation scenarios: raising roof albedo and increasing urban irrigation. The mitigation scenarios are compared to the control scenario. Within the cool roof scenario, roof albedo is raised from 0.20, its value in the control scenario, to 0.60, following Cao et al. [2015]. For the irrigation scenario, we activate the WRF irrigation scheme, inactive in the control case, which causes the top two model layers to reach critical moisture content such that transpiration is not limited by water availability. The WRF irrigation scheme is implemented at 21:00 local standard time (LST) every day from May to September. The WRF irrigation scheme is essentially equivalent to a city actively watering all unpaved areas each evening.

3. Results and Discussion

3.1. Evaluation of Heat Island Mitigation Strategies

We use 2-m temperature simulations from WRF-SLCUM to evaluate the impact of heat island mitigation strategies. To check the performance of WRF using this set-up, we compare WRF-simulated near-surface (2-m) temperature with observations and the results are shown in the supplemental Figure S2. Overall, WRF simulations are well-correlated with observed temperature yielding values of 0.82 and 0.76 for the coefficient of determination (i.e., r^2) during normal and heat wave episodes, respectively. We found that average (i.e., arithmetic mean) temperatures across KCMA during both normal and heatwave conditions were sensitive to elevation, with lower elevations having higher temperatures; for example, compare the temperature maps in Figure 2a,b to elevation map in Figure 1b. However, the spatial patterns of temperature reductions from the two mitigation scenarios, for both normal and heat wave episodes, match the land-use type distribution; see the larger temperature reductions (Figure 2c-f) correlate with the higher density development land-use types (Figure 1c). We note, though, that most of the high

intensity development is located near the river and at low elevation relative to the surrounding areas, thus the influence on temperature mitigation strategies of land-use type cannot be fully separated from the influence of topography.

The average daytime (07:00 – 19:00 LST) temperature reductions from the mitigation scenarios varies by urban development intensity (Figure 3). For the roof albedo scenario, the average temperature reduction for the normal episode ranges from 0.07 to 0.17 °C depending on the development intensity. For the heat wave episode, the temperature reduction varies from 0.01 to 0.09 °C, showing somewhat reduced mitigation effect compared to that of the normal episode (Figure 3a). This result is different from that reported in Cao et al. [2015] where they reported significantly larger temperature reductions from cool roofs during heat waves compared to normal summer conditions. The absence of increased temperature reductions during heatwaves in this work counters the generalization of a simple hypothesis that could be derived from Cao et al. [2015]: that urban mitigation strategies will produce larger temperature reductions given higher initial temperatures. This indicates that the geography of the city and regional meteorology conditions influences the performance of mitigation strategies during extreme conditions such as heatwaves relative to their performance during normal conditions. We expand this discussion in later sections.

Temperature reductions from the urban irrigation scenario (Figure 3b) are consistently larger than those of the roof albedo scenario for all development intensity types with mean temperature reductions being equal to or larger than 0.2 °C for all cases. As shown in Figure 3b, the interquartile ranges (IQR, or difference between upper and lower quartiles) for the normal and heat wave episodes overlap, suggesting that there is no significant difference in the effect of temperature reductions between the normal and heat wave episodes.

We applied the nonparametric Wilcoxon-Mann-Whitney test (WMW) [Mann and Whitney, 1947] to decide whether there is a statistically significant difference in the mean temperature between the control and mitigation scenarios. Using the WMW test, we can evaluate whether the population distributions are identical without normality assumptions for the data. For this test, we assumed that each of the control and mitigation scenarios is an independent group for which we can estimate the mean air temperature. Our assumption of independent grouping between control and mitigation scenarios is similar to the case to examine whether there is a difference in simulated mean temperature from a climate model due to different scenarios about atmospheric CO_2 concentration levels [Wilks, 2011]. Note that we used this nonparametric test because the temperature distribution may not be normally distributed across the study region. As indicated by the IQR in the boxplots of Figure 3, the Wilcoxon-Mann-Whitney test determined that, except for the roof albedo scenario during the heat wave episode, the temperature in each mitigation scenario was significantly different from that in the control case (p-value much less than 0.05). A significant result indicates that those mitigation cases were effective in cooling air temperature in KCMA.

Figure 3a shows that the mean daytime temperature reductions from the cool roof scenario across KCMA are 0.08 and 0.02 °C for the normal and heat wave episodes, respectively. The magnitude of temperature reductions from our cool roof simulation is smaller than those of Cao et al. [2015] and Vahmani et al. [2016]. However, we note that air temperature depends on many factors

including the land surface conditions (e.g., level of urbanization) and influence from outside the urban area (e.g., sea breeze) as well as the assumption about the cool roof albedo. For example, Vahmani et al. [2016] reported a daytime temperature reduction of 0.9 °C from the adoption of cool roofs in Southern California which is based on a higher area ratio for the industrial/commercial area (33%) with a higher cool roof albedo of 0.85 than our study area. We note that although the land classification method of our study does not exactly match that of Vahmani et al. [2016], our high development area accounts for only 5% of KCMA, which is much smaller than the industrial/commercial area (~30%) used in Vahmani et al. [2016]. Cao et al. [2015] showed that the temperature reduction from a similar cool roof scenario was larger during the heat wave episodes than during the normal episodes while our results shows a higher temperature reduction during the normal periods than the heat wave. Possible reasons for this are discussed in section 3.3.

The cooling effects of irrigation on daytime (07:00 – 19:00 LST) temperatures are evident over all three urban types for both the normal and heat wave episodes (Figure 3). The decrease in the air temperature from urban irrigation is largely due to increased evaporation. The mean temperature reduction for the normal episodes ranges from 0.21 to 0.29 °C while the heat wave episodes also show a similar range of temperature reduction (0.20 - 0.29 °C). The urban irrigation reduced average daytime temperatures across KCMA by 0.28 and 0.26 °C for the normal and heat wave episodes, respectively (Figure 3b). The high development area had the lowest effect of the irrigation strategy on the temperature reduction.

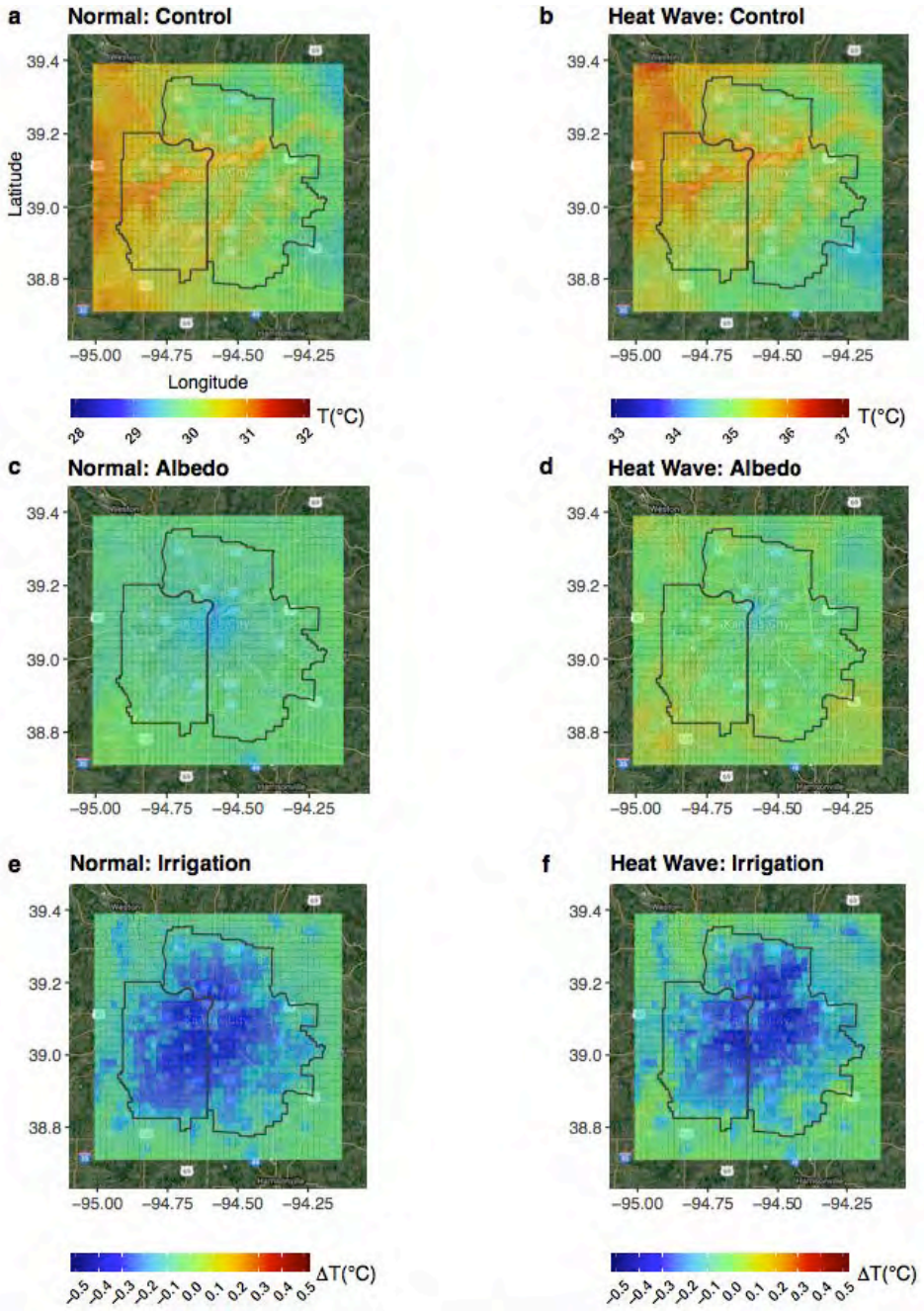

Figure 2. (a, b) Simulated average daytime (07:00 – 19:00 LST) 2-meter air temperature. (c-f) Temperature difference (°C, mitigation minus control) due to roof albedo and urban irrigation mitigation scenarios for the normal and heat wave episodes.

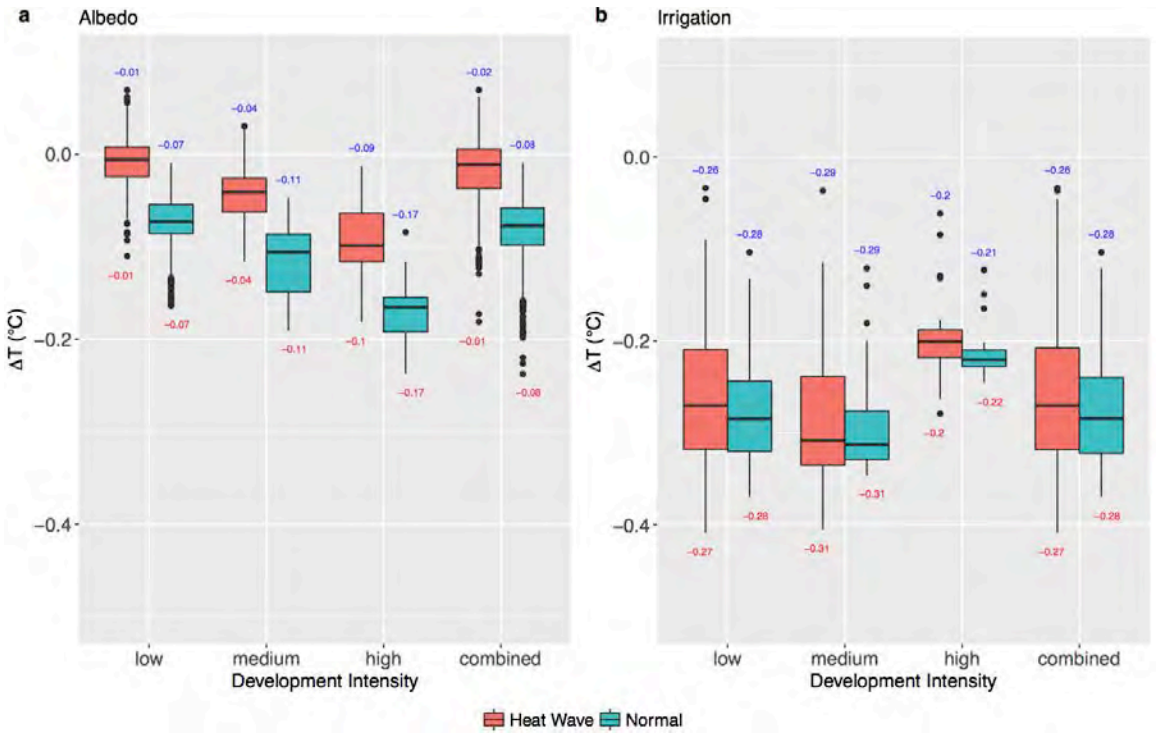

Figure 3. Boxplots of simulated daytime (07:00 – 19:00 LST) air temperature differences (ΔT, mitigation minus control) for (a) roof albedo, and (b) urban irrigation. For each scenario, the boxplot is shown for the low, medium and high development areas and the entire KCMA (i.e., "combined"). The numbers at the top (blue) and bottom (red) of the box represent mean and median values of the data, respectively.

To provide a more complete picture of the statistical distribution of the simulated temperature differences from the adoption of different mitigation strategies, we show histograms of temperature changes where the relative amount of data (i.e., number of grid cells in the modeling domain) for each development type and the range of data values from individual model grid cells. Figure 4 shows histograms for daytime temperature changes (ΔT, mitigation minus control) from all mitigation scenarios by development intensity for both the normal and heat wave episodes. For the roof albedo scenario, the high development intensity area shows the largest temperature reduction (i.e., ΔT) for both the normal and heat wave episodes. This result is expected because the high development area, on average, is associated with a larger roof area ratio within a given pixel. Also, the range of ΔT in the high development area is larger than those of the medium and low development areas, showing larger variability in temperature reductions.

In KCMA, the low development area has low roof area fractions (<10%). For both the normal and heat wave episodes, the high development density area shows the smallest temperature reduction from urban irrigation (Figure 4). This is likely because low and medium development areas have larger available irrigated (urban vegetation) areas than those of the high development intensity area when we use the same irrigation scheme across the development intensity types. This result suggests that at the regional level the mitigation benefits from urban irrigation may be maximized when focusing more on the low and medium development intensity areas for which irrigation strategies can be implemented relatively easily compared to the high development area.

For some cases (e.g., medium development for the albedo scenario during the normal episodes), the distribution of ΔT is bimodal, suggesting that there is spatial variability in the effect of mitigation strategies within the same development intensity, perhaps depending on land surface conditions and local atmospheric conditions. Characterizing this spatial variability with a similar development level through future studies would help planning detailed mitigation plans. Additional detailed land cover classification could be useful in understanding the urban heat island and evaluating the mitigation strategies applied.

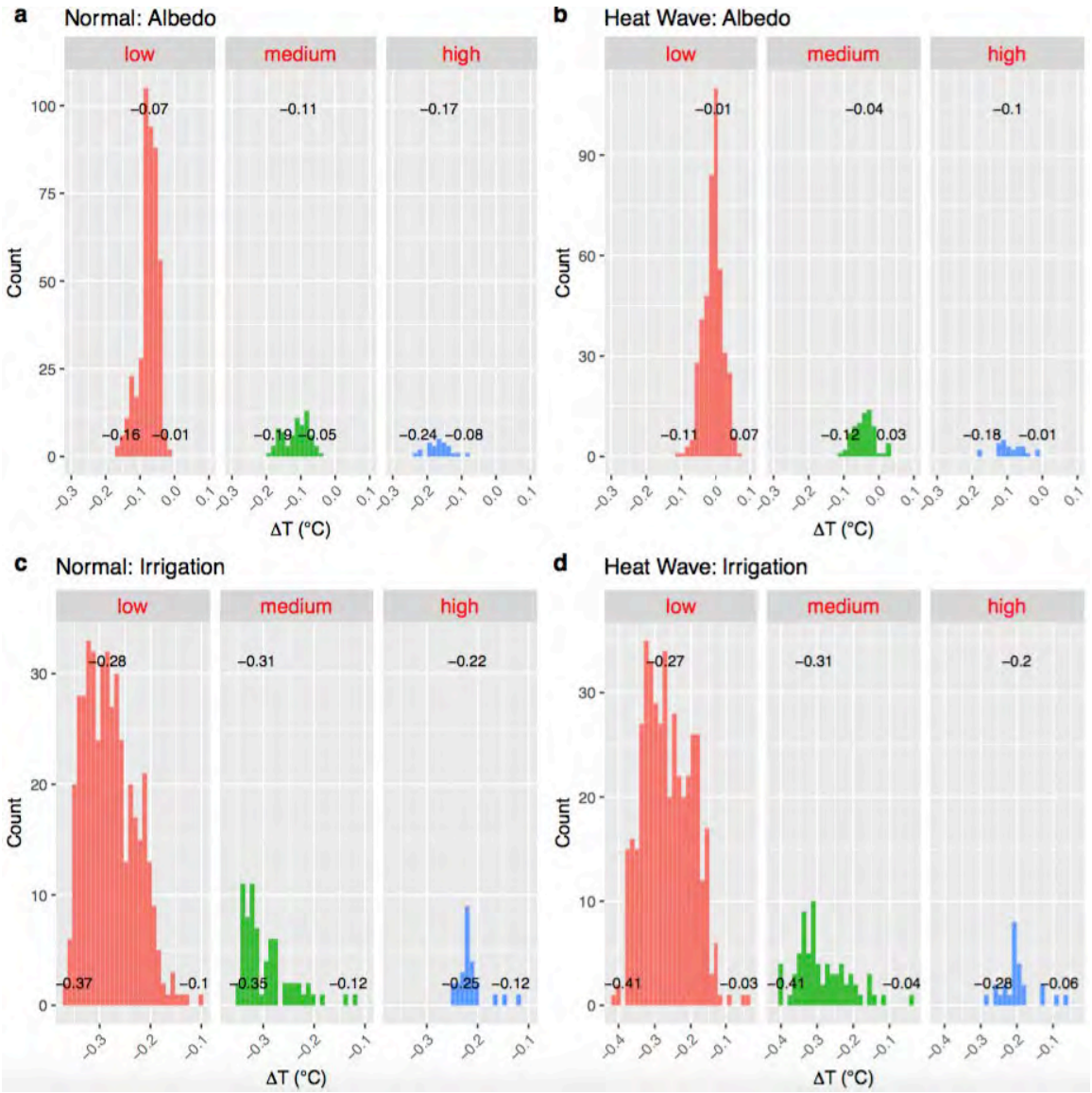

Figure 4. Histogram of daytime (07:00 – 19:00 LST) temperature differences (°C) by mitigation scenario for the normal (a and c) and heat wave (b and d) episodes. "Albedo" and "Irrigation" in the plot titles denote the cool roof albedo and urban irrigation mitigation scenarios, respectively. The numbers at the bottom of each plot represent the minimum and maximum ΔT values within the boundary of KCMA. The number at the top of each plot shows the median ΔT values.

3.2. Diurnal Cycles of Mitigation Effects

Cool roofs and urban irrigation produce different diurnal patterns of cooling in KCMA (Figure 5, Supplemental Figures S3 – S6). During normal episodes, cool roofs provide peak cooling during the middle of the night, whereas urban irrigation provides the most cooling during the daylight hours. During heat waves, we see the largest cooling impacts during early morning hours prior to sunrise. During heat waves we see increased temperatures under both the cool roof and urban irrigation scenarios during the late afternoon and early evening hours. Both the later afternoon temperature increases and the early morning temperature reductions are potentially related to changes in local meteorological patterns including a decrease in precipitation that was found in the cool roof mitigation scenario during the heat wave episodes. We discuss this precipitation effect further in Section 3.3.

Urban irrigation (irrigated at 21:00 LST) reduces temperatures reduction more during the daytime and evening than the early morning (Figure 5). This is likely due to irrigation induced evaporation peaking with large available surface energy during the daytime, which lowers the air temperature. The low temperature reduction from urban irrigation during the early morning hours, in particular for the normal case, is consistent with the result in Vahmani and Ban-Weiss [2016] where they reported warming during the nighttime relative to the daytime due to increased nocturnal upward ground heat fluxes.

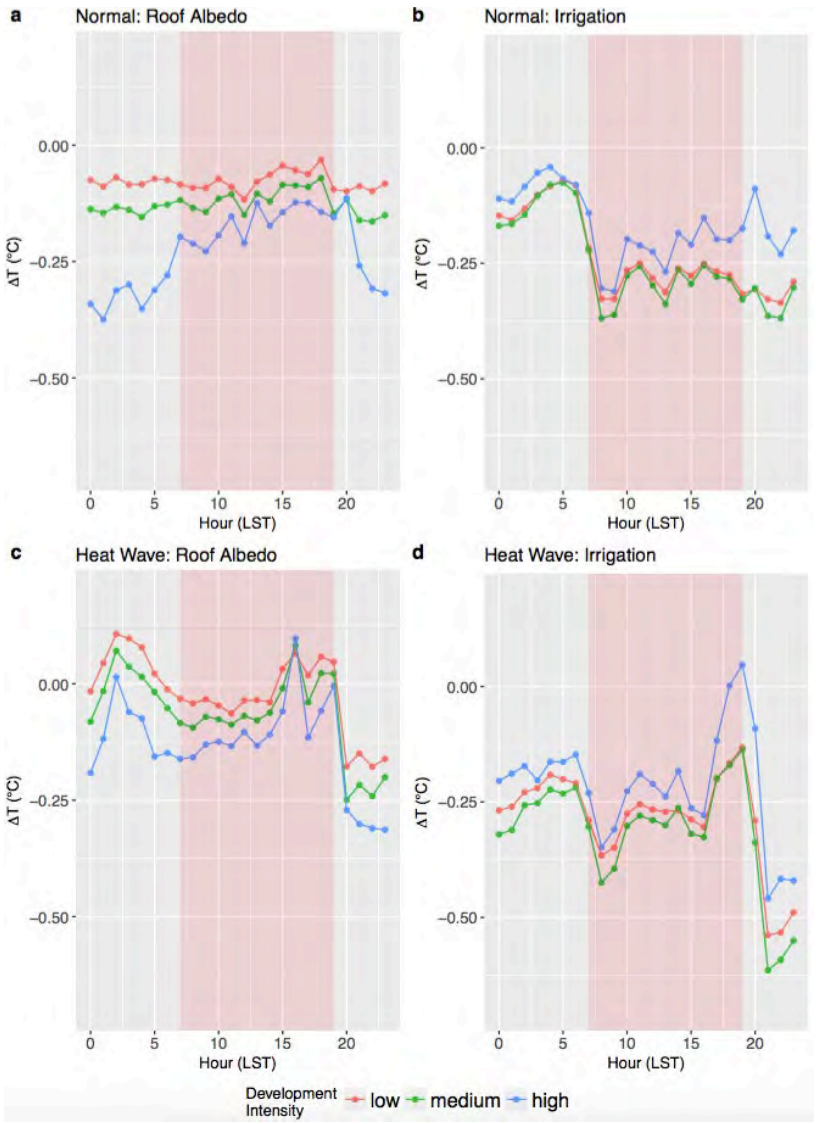

Figure 5. Diurnal cycles of differences in the air temperature (ΔT, mitigation – control) for the mitigation strategies during the normal (a and b) and heat wave (c and d) episodes. The shaded region in light red shows the hours of sunlight (07:00 – 19:00 LST).

3.3. Impact of Mitigation Strategies on Local Weather

We found that during heat waves the cool roof scenario showed higher air temperature than the control case during early evening hours (15:00 – 19:00 LST) (Figure 5c). Figure 6a shows the simulated average air temperature for the control case and the cool roof albedo scenario during 15:00 – 19:00 LST hours of the heat wave episodes. In Figure 6a, the average air temperature is higher in the cool roof albedo scenario than in the control case, which was also shown in the diurnal cycle of ΔT for the cool roof scenario during the heat wave episodes (Figure 5c). We explored a few meteorological variables related to air temperature and found that simulated

precipitation is reduced in the cool roof scenario during 15:00 – 19:00 LST hours of the heat wave episodes (Figure 6b), likely causing the corresponding increase to air temperature. When the surface is moist due to the increased precipitation, latent heat flux also increases, reducing air temperature (Figure 6c). It is possible that this change in precipitation is an artifact of the WRF modeling, as preliminary analysis indicates that the control scenario has a higher frequency of late afternoon/early evening precipitation than is observed. Also, it is possible that these changing meteorological conditions also impact the early morning temperature reductions seen in the mitigation scenarios during heat waves. These changes to local meteorological patterns are interesting and further study could potentially improve our understanding of how urban form interacts with local meteorological patterns.

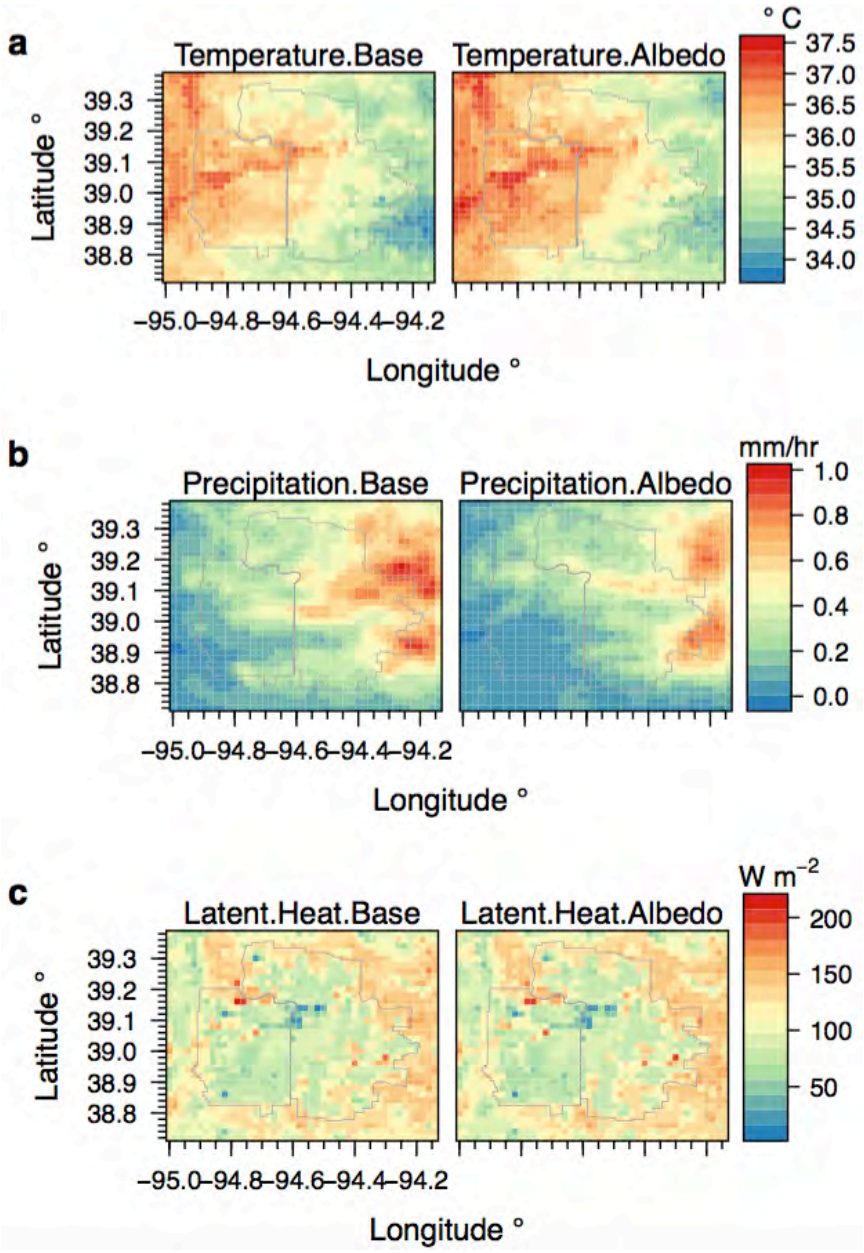

Figures 6. Comparison of early evening (15:00 – 19:00 LST) mean air temperature (a), non-convective precipitation (b) and latent heat (c) between the control case and the roof albedo scenario during the heat wave episodes. “base” and “albedo” denotes the control and cool roof albedo cases, respectively.

3.4. Research and Policy Implications

Using high-resolution meteorological simulations, we have shown that a policy of enhancing roof albedo by 0.4 in KCMA could reduce regional average daytime (7:00 – 19:00 LST) temperatures by 0.08 and 0.02 °C for the normal summer conditions and heat wave episodes, respectively, showing different mitigation impacts on temperature reduction depending on the land development type. We also found that during heatwaves, temperature reductions might be larger during the early morning hours, but that a few hours of increased temperature might occur during the late afternoon and early evening as a result of decreased precipitation. These particular patterns found during heatwaves deserve additional study due to uncertainty about the interaction between cool roofs and precipitation patterns.

These results suggest that regions with relatively low roof area fractions such as KCMA may benefit from reflective cool roofs only marginally although the benefit for the high development area is higher than the regional average. Recall that for KCMA, the majority of the region is low development area (82%), which has low roof area fractions (<10%), and this further reduces the impact of reflective cool roofs on temperature reduction. Compared to the reflective cool roof scenario, however, the urban irrigation scenario showed significantly larger temperature reductions, with average daytime temperatures reductions of 0.28 and 0.26 °C for the normal and heat wave episodes, respectively. These results suggest that for regions with low roof fractions urban irrigation may be a more efficient policy to be adopted to mitigate urban heat island than reflective cool roofs although reflective cool roof can be still effective in localized areas with high development density. We note, however, that these results presume all roofs are available for albedo modification and there exists ample water availability for urban irrigation.

References

Akbari, H., Konopacki, S., and Pomerantz, M. (1999), Cooling energy savings potential of reflective roofs for residential and commercial buildings in the United States. Energy 24 (5), 391−407.

Bagley, J. E., et al. (2017), Assessment of an atmospheric transport model for annual inverse estimates of California greenhouse gas emissions, J. Geophys. Res. Atmos., 122, doi:10.1002/ 2016JD025361.

Bretherton, C. S. and Park, S. (2009), A New Moist Turbulence Parameterization in the Community Atmosphere Model. J. Climate, 22, 3422–3448, doi: 10.1175/2008JCLI2556.1.

Chen, F. and Dudhia, J. (2001), Coupling an advanced land surface- hydrology model with the Penn state-NCAR MM5 modeling system: I. Model implementation and sensitivity, Mon. Weather Rev., 129 569–85

Chen, F., et al. (2011) The integrated WRF/urban modelling system: development, evaluation, and applications to urban environmental problems. Int J Climatol 31:273–288.

Ching, J., et al. (2009), National Urban Database and Access Portal Tool (NUDAPT), Bulletin of American Meteorological Society, 90(08), 1157-1168.

Li, D., Bou-Zeid, E. and Oppenheimer, M. (2014), The effectiveness of cool and green roofs as urban heat island mitigation strategies, Environ. Res. Lett. 9, 055002, doi:10.1088/1748-9326/9/5/055002

Dudhia, J. (1989), Numerical study of convection observed during the Winter Monsoon Experiment using a mesoscale two dimensional model, J. Atmos. Sci., 46, 3077–3107.

Georgescu, M., Morefield, P. E., Bierwagen, B. G., and Weaver, C. P. (2014),Urban adaptation can roll back warming of emerging megapolitan regions. Proc. Natl. Acad. Sci. U. S. A. 111 (8), 2909−2914.

Grell, G. A. and Freitas, S. R. (2014), A scale and aerosol aware stochastic convective parameterization for weather and air quality modeling, Atmos. Chem. Phys., 14, 5233-5250, doi:10.5194/acp-14-5233-2014.

Hassid, S. et al. (2000), The effect of the Athens heat island on air conditioning load Energy Build., 32, 131–41.

Jeong, S., et al. (2016), Estimating methane emissions in California's urban and rural regions using multi-tower observations, J. Geophys. Res. Atmos., 121, 13,031-13,049, doi:10.1002/2016JD025404.

Jeong, S., et al. (2017), Estimating methane emissions from biological and fossil-fuel sources in the San Francisco Bay Area, Geophys. Res. Lett., 44, 486–495, doi:10.1002/2016GL071794.

Kusaka H, Kondo, H, Kikegawa, Y and Kimura, F. (2001), A simple single layer urban canopy model for atmospheric models: comparison with multi-layer and slab models Bound.-Layer Meteorol., 101 329–58.

Kusaka, H. and Kimura, F. (2004), Coupling a single-layer urban canopy model with a simple atmospheric model: impact on urban heat island simulation for an idealized case J. Meteorol. Soc. Japan 82 67–80.

Levinson, R., Akbari, H., Konopacki, S., and Bretz, S. (2005), Inclusion of cool roofs in nonresidential Title 24 prescriptive requirements. Energy Policy 33, 151−170.

Levinson, R., and Akbari, H. (2010), Potential benefits of cool roofs on commercial buildings: conserving energy, saving money, and reducing emission of greenhouse gases and air pollutants. Energy Efficiency, 3 (1), 53−109.

Li, D and Bou-Zeid, E. (2013), Synergistic interactions between urban heat islands and heat waves: the impact in cities is larger than the sum of its parts J. Appl. Meteorol. Climatol. 52 2051–64.

Li, D., and E. Bou-Zeid (2014), Quality and sensitivity of high-resolution numerical simulation of urban heat islands, Environ. Res. Lett., 9, 055001.

Luber, G. and McGeehin, M. (2008), Climate change and extreme heat events. Am. J. Prev. Med., 35(5), 429−435.

Mann, H. B. and Whitney, D.R. (1947), On a test of whether one of two random variables is stochastically larger than the other, Annals of Mathematical Statistics, 18, 50-60.

Mesinger, F., et al. (2006), North American regional reanalysis, Bull. Am. Meteorol. Soc., 87, 343–360, doi:10.1175/BAMS-87-3-343.

Mid-America Regional Council (2017), GIS Datasets, http://www.marc.org/Data-Economy/Maps-and-GIS/GIS-Data/GIS-Datasets (accessed in January 2017).

Miller, N. L., Hayhoe, K., Jin, J., and Auffhammer, M. (2008), Climate, extreme heat, and electricity demand in California. Journal of Applied Meteorology and Climatology, 47, 1834−1844.

Millstein, D. and Menon, S. (2011), Regional climate consequences of large-scale cool

roof and photovoltaic array deployment Environ. Res. Lett. 6, 034001.

Mlawer, E. J., Taubman, S. J., Brown, P. D., Iacono, M. J., and Clough, S. A. (1997), Radiative transfer for inhomogeneous atmospheres: RRTM, a validated correlated-k model for the longwave, J. Geophys. Res., 102, 16,663–16,682, doi:10.1029/97JD00237.

Morrison, H., Thompson, G. and Tatarskii, V. (2009), Impact of cloud microphysics on the development of trailing stratiform precipitation in a simulated squall line: Comparison of oneand two-moment schemes. Mon. Wea. Rev., 137, 991–1007, doi:10.1175/2008MWR2556.1.

National Centers for Environmental Information (2017), The Integrated Surface Database, https://www.ncdc.noaa.gov/isd (accessed in January 2017).

National Map (2017), National Elevation Data, https://nationalmap.gov/elevation.html (accessed in January 2017).

Nazaroff, W. W. (2013), Exploring the consequences of climate change for indoor air quality Environ. Res. Lett. 8 015022, doi:10.1088/1748-9326/8/1/015022.

Parker, D. S. and Barkaszi, S. F. (1997), Roof solar reflectance and cooling energy use: field research results from Florida. Energy Build. 25, 105−115.

Salamanca F, Georgescu, M., Mahalov, A., Moustaoui, M., Wang, M. and Svoma, B. M. (2013), Assessing summertime urban air conditioning consumption in a semiarid environment Environ. Res. Lett. 8 034022

Skamarock, W. C., et al. (2008), A description of the advanced research WRF Version 3, NCAR Tech. Note NCAR/TN-475 + STR, doi:10.5065/D68S4MVH.

Vahmani, P., and Hogue, T. S. (2015), Urban irrigation effects on WRF-UCM

summertime forecast skill over the Los Angeles metropolitan area, J. Geophys. Res. Atmos., 120, 9869–9881, doi:10.1002/2015JD023239.

Vahmani, P., and Ban-Weiss, G. (2016), Climatic consequences of adopting drought-tolerant vegetation over Los Angeles as a response to California drought, Geophys. Res. Lett., 43, 8240–8249, doi:10.1002/2016GL069658.

Vahmani, P., Sun, F., Hall, A. and Ban-Weiss, G. (2016), Investigating the climate impacts of urbanization and the potential for cool roofs to counter future climate change in Southern California, Environ. Res. Lett. 11 (124027), doi:10.1088/1748-9326/11/12/124027.

Wilks, D. S. (2011), Statistical methods in the atmospheric sciences. Oxford: Academic Press, pp. 704.

Yang, J., et al. (2013), Impact of heat wave in 2005 on mortality in Guangzhou, China. Biomed. Environ. Sci. 26, 647−654.

Appendix

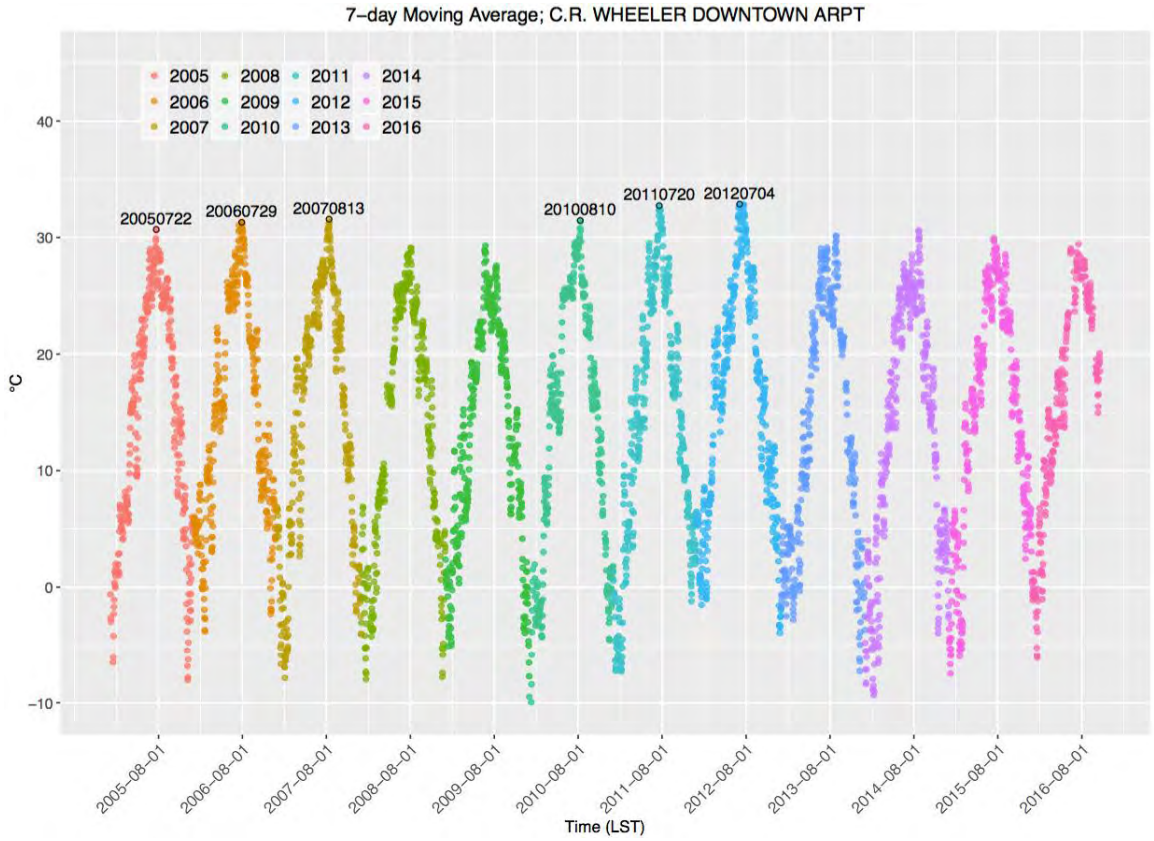

Figure S1. Seven-day moving average for daily temperature (plotted at the center date) at C. R. Wheeler Airport in Kansas City, MO. The black open circles represent the center date of each identified heat wave spanning seven days.

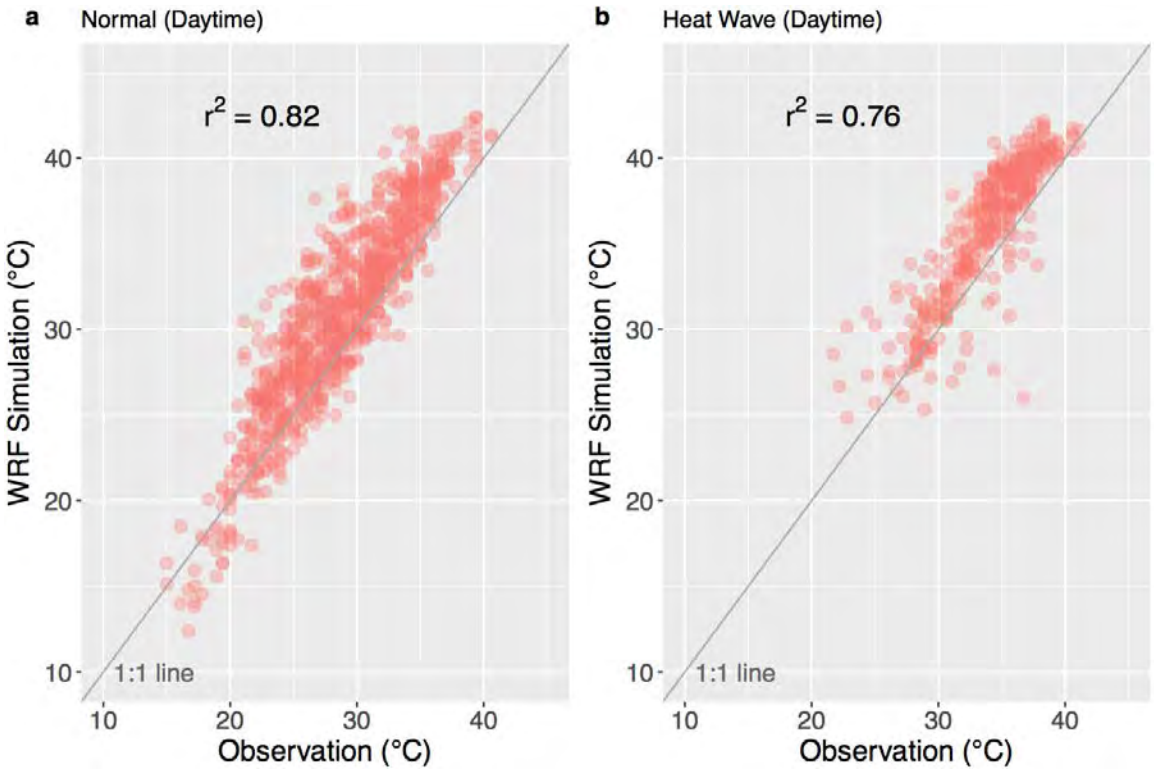

Figure S2. Comparison of temperature between WRF simulations and observations at C. R. Wheeler Airport in Kansas City, MO. The data points shown in the plots represent all hourly data during normal (10 weeks) and heat wave (6 weeks) episodes.

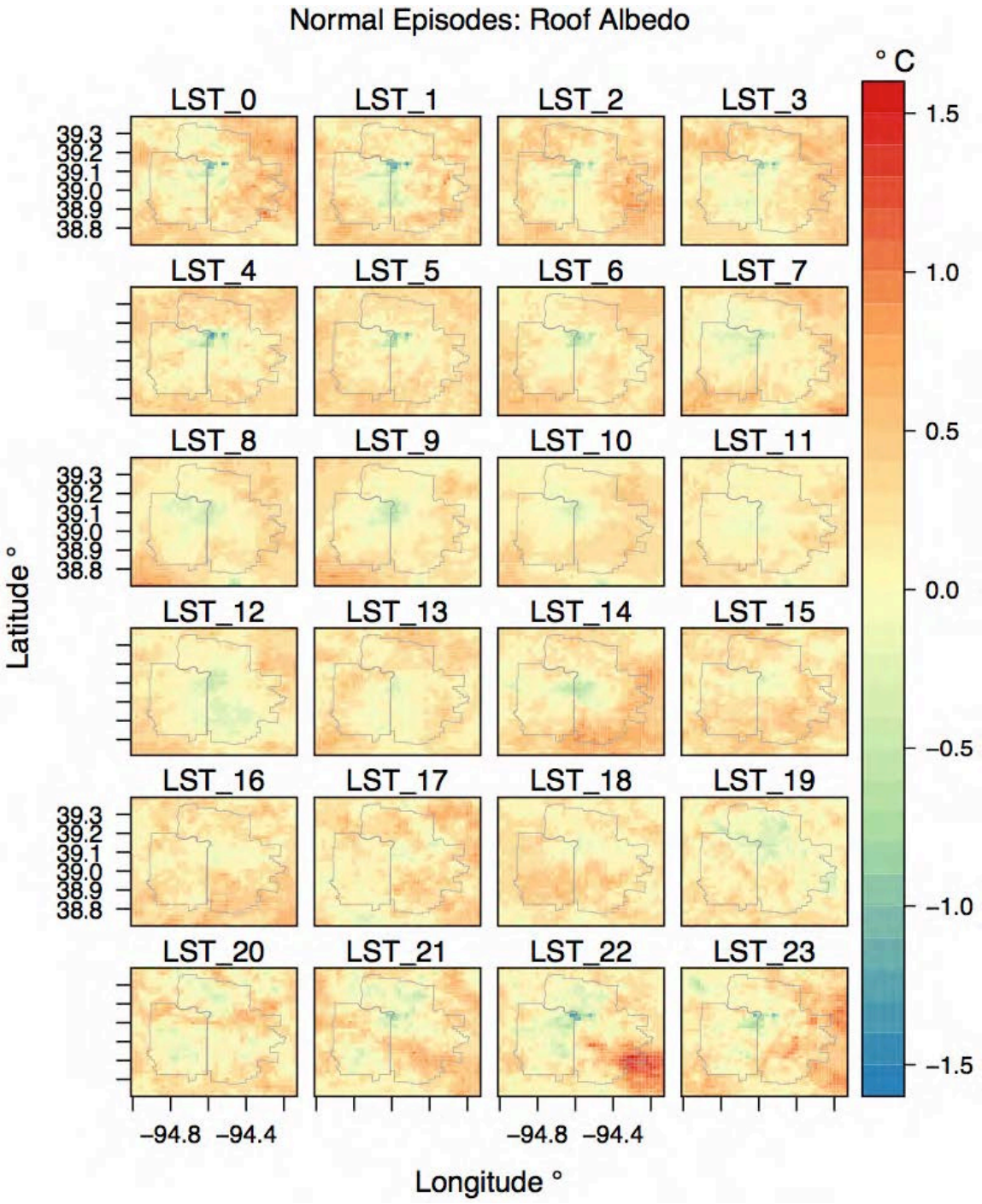

Figure S3. Diurnal cycles of change in temperature (mitigation – control, °C) for the normal episode based on the cool roof mitigation scenario.

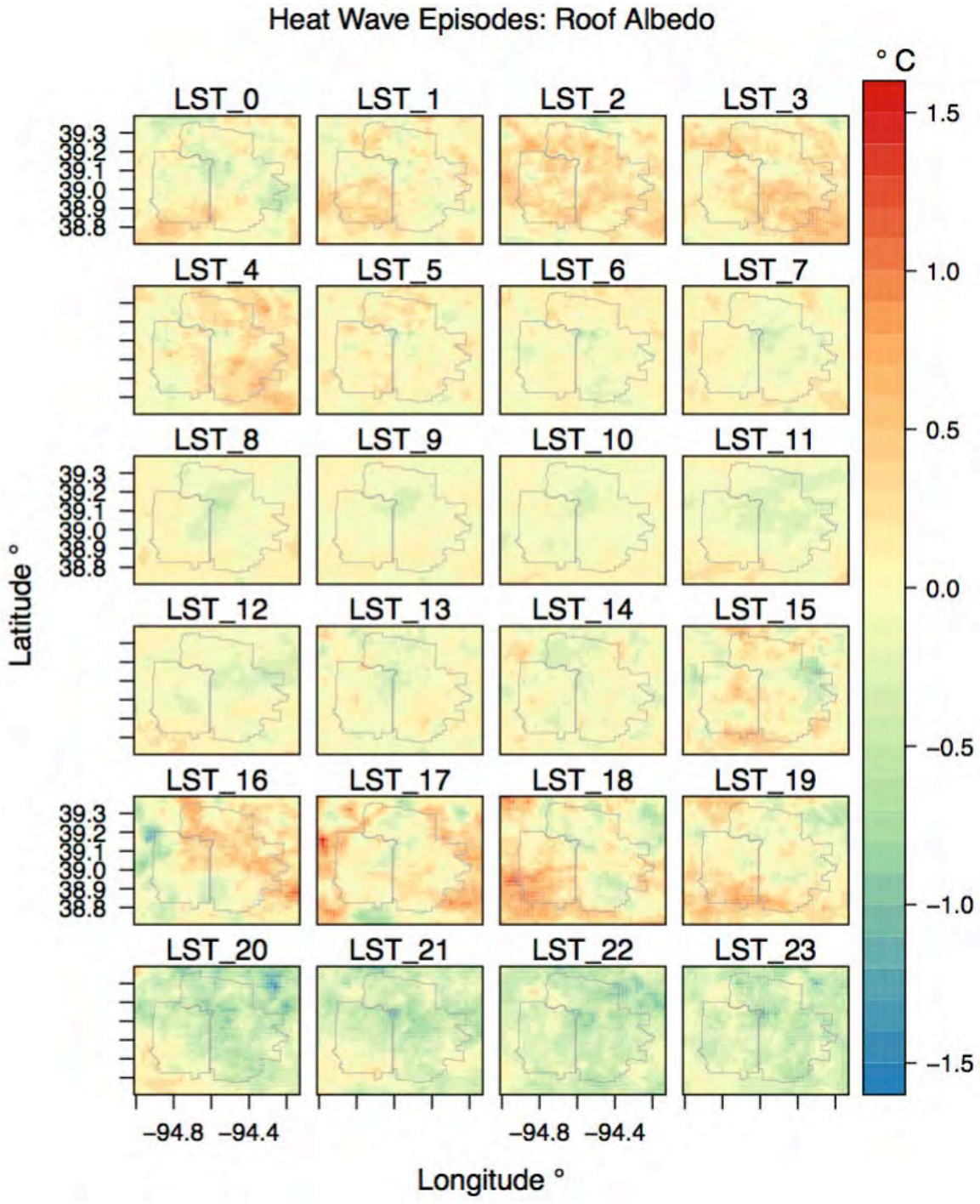

Figure S4. Diurnal cycles of change in temperature (mitigation – control, °C) for the heat wave periods based on the cool roof mitigation scenario.

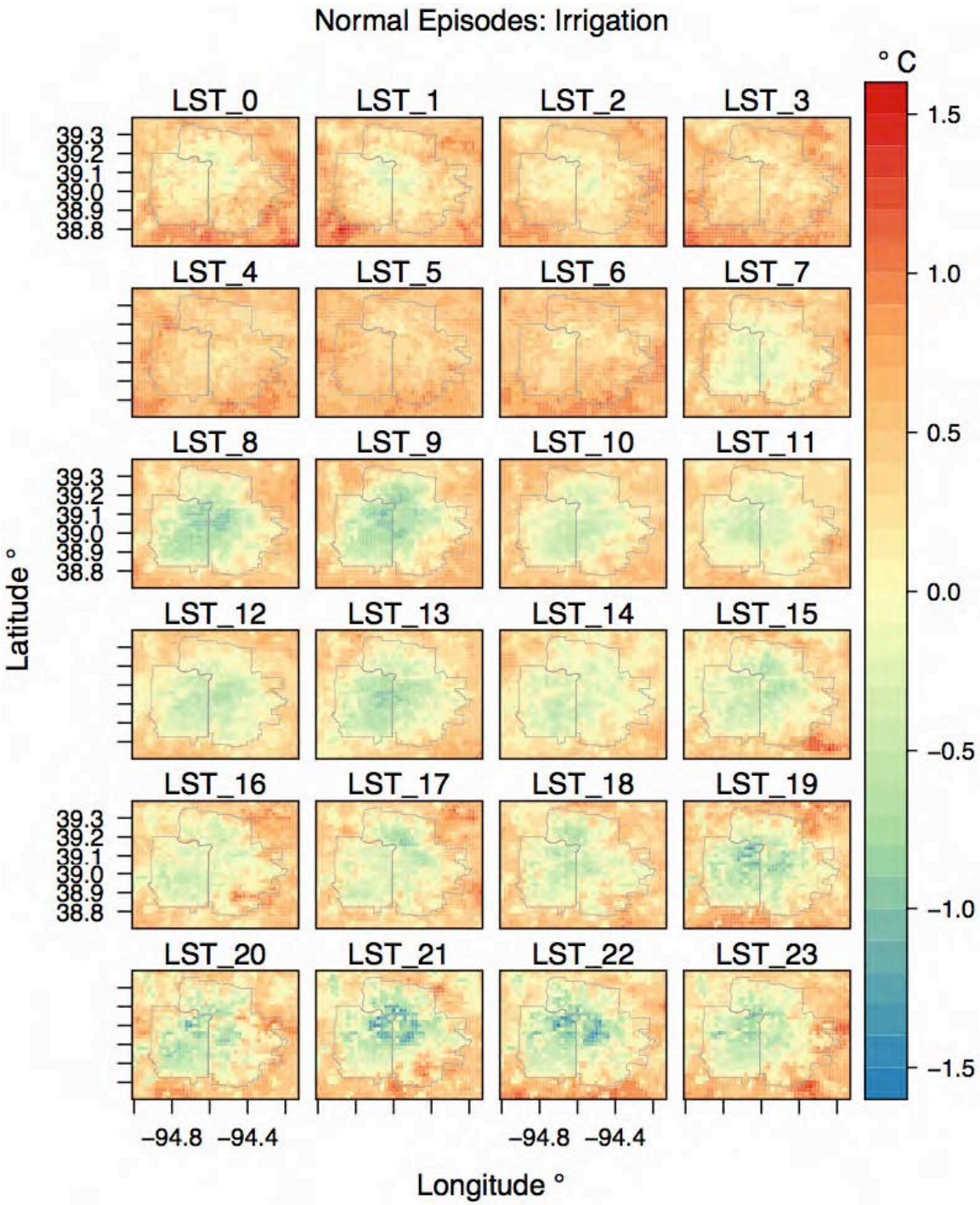

Figure S5. Diurnal cycles of change in temperature (mitigation – control, °C) for the normal episode based on the urban irrigation mitigation scenario.

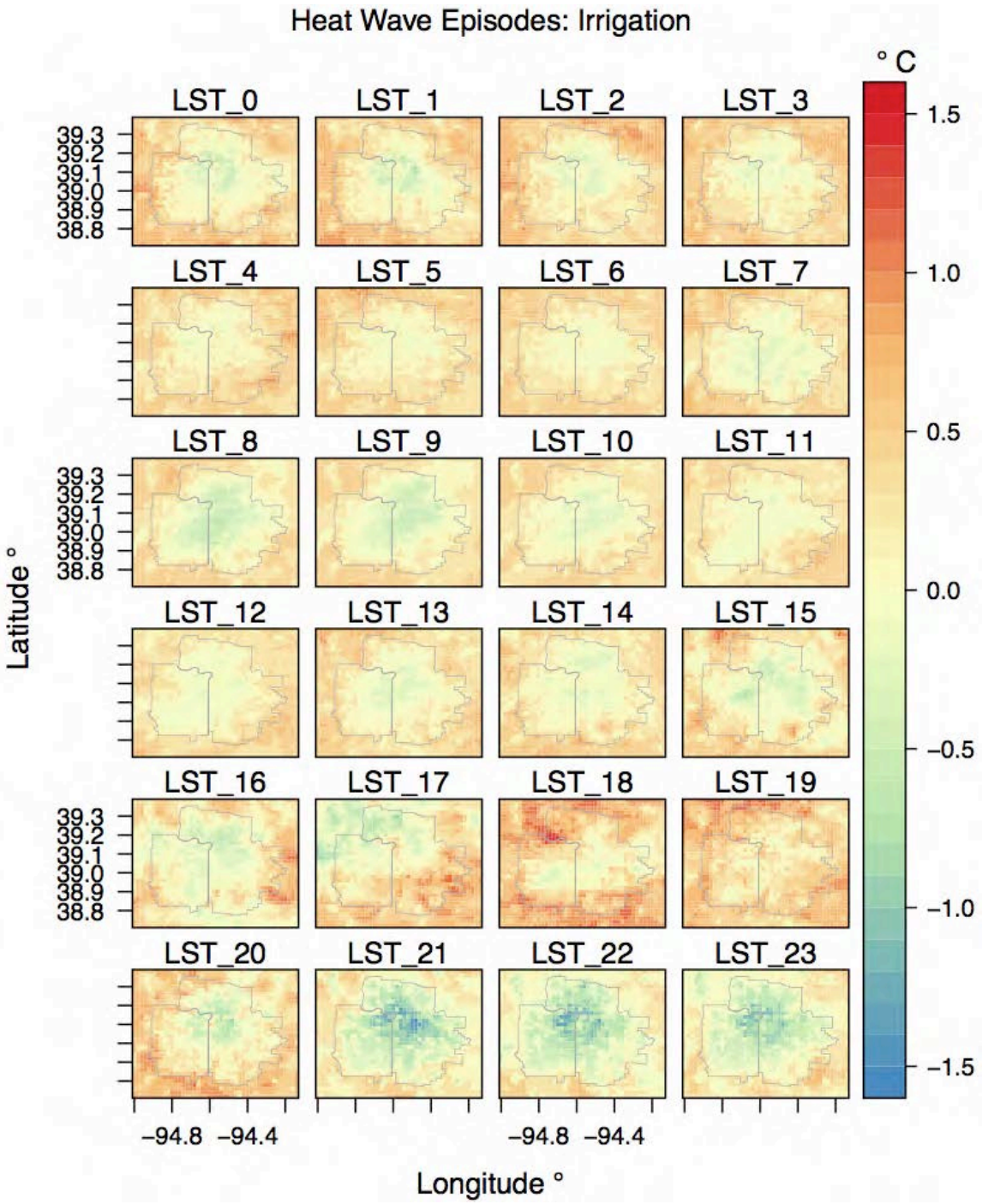

Figure S6. Diurnal cycles of change in temperature (mitigation – control, °C) for the heat wave periods based on the urban irrigation mitigation scenario.